Climatological Characteristics of Fog at Cape Town International Airport

LYNETTE VAN SCHALKWYK

Department of Geography, Geoinformatics and Meteorology, University of Pretoria, Pretoria, and eTV (Pty) Ltd., Cape Town, South Africa

LIESL L. DYSON

Department of Geography, Geoinformatics and Meteorology, University of Pretoria, Pretoria, South Africa

(Manuscript received 14 February 2012, in final form 11 January 2013)

ABSTRACT

The character of fog at Cape Town International Airport (CTIA), South Africa, is investigated, using 13 yr of historical hourly data during the period 1997–2010. Hourly surface observations are used to identify fog types that most frequently affect CTIA, by using an objective fog-type classification method that classifies fog events according to their primary formation mechanisms. Fog-type characteristics, such as the minimum visibility, duration, and time of onset and dissipation, are determined. Self-organizing maps (SOMs) are used to determine the dominant synoptic circulation types associated with fog at CTIA. Results show that radiative processes are the most common cause of fog, with an enhanced likelihood of radiation fog in winter. Cloud-base-lowering fog and advection fog events are more likely at the start of the fog season. As the fog season (March–August) progresses, synoptic circulations associated with fog change from a dominant low pressure pattern along the west coast in March and April to a dominant interior high pressure pattern toward July and August. The techniques presented may be used to provide aviation forecasters with a detailed description of the types of fog that frequently occur, their characteristics, and the synoptic circulation associated therewith.

1. Introduction

The reduced ceiling and horizontal visibility associated with fog is of particular importance for the aviation industry. Safety is a considerable concern to the aviation community and accidents often occur in reduced visibility conditions (Tardif and Rasmussen 2007). According to the International Civil Aviation Organization (ICAO), takeoff and landing of aircraft under visual flight rules (VFR) is not allowed when the visibility is less than 5000 m and the cloud-base height is 457 m (1500 ft) or less. These rules are adjusted according to the experience of the pilot, the type of aircraft, and the instrumentation at an airport. For instance, at Cape Town International Airport (CTIA), South Africa, with a category IIIB Instrument Landing System (ILS), aircraft with suitable equipment and qualified pilots can land with a minimum runway visual range (RVR) between 75 and 200 m and 0-m decision height, or a cloud base and vertical visibility of 0 m (Civil Aviation Authority 2007).

In South Africa, the highest fog frequencies occur along the west coast where fog is observed on more than 50 days yr^{-1}on average (Olivier and Van Heerden 1999). They determined that sea surface temperatures along the west coast vary between 13° and 15°C and with the arid, hot land surface, advection fog occurs almost exclusively and throughout the year. The fog season at CTIA falls between March and August when at least 1 day of fog occurs per month. The month with the highest frequency of fog (3.5 days) is May (Van Schalkwyk 2011) and fog generally occurs most frequently during winter, which is also the rainy season (SAWB 1968).

CTIA has an elevation of 46 m above sea level and is situated on the extreme southern part of the west coast of South Africa. The airport is situated on the Cape Flats, which, as its name suggests, is a fairly level stretch of land that is part of the coastal plain and is approximately 45 km wide at the latitude of the airport. Cape Town is situated approximately 13 km northwest of the airport and False Bay is 12 km to its south (Fig. 1). CTIA

Corresponding author address: Lynette van Schalkwyk, Dept. of Geography, Geoinformatics and Meteorology, Private Bag X20, Hatfield 0028, South Africa.
E-mail: lynvanschalkwyk@gmail.com

DOI: 10.1175/WAF-D-12-00028.1

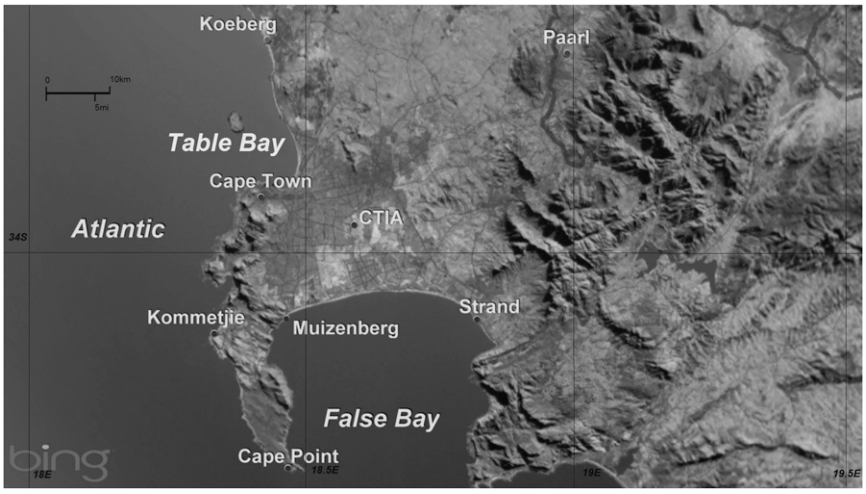

FIG. 1. Map showing the location of CTIA at 33.9694°S and 18.5972°E, with the Atlantic Ocean to its west, False Bay to its south, and a mountain range to the east (MeteoGraphics 2010).

forms part of the greater southwestern Cape region, which receives its maximum rainfall in winter, from May to August. It is the airport with the greatest number of fog days in South Africa (SAWB 1968). Due to the influence of the cold Benguela Current, west coast fog is often advected inland with a northwesterly wind, affecting CTIA as either low-based stratus or in some cases fog (SAWS 2010). A synoptic circulation type frequently associated with fog at CTIA is the coastal low (SAWB 1968). The coastal lows that occur along the South African coastal belt are local shallow systems associated with intense and rapid weather changes. The development of the coastal low depends on synoptic-scale flow off the interior toward the coast and out to sea and is often an extension of the surface trough. The weather changes associated with a coastal low always occur in the form of a change in wind direction and speed, and a temperature change from relatively hot to cool postlow conditions. These weather changes may be accompanied by low cloud, fog, or drizzle (Carter 2005).

In terms of air traffic movements CTIA is the second busiest airport in South Africa after O. R. Tambo International Airport (Johannesburg), and the third largest in Africa (World Airports 2010). In 2009, there were nearly 48 000 aircraft arriving at the airport and it hosts more than 15 international airlines (ACSA 2010). With a category IIIB ILS, weather-related diversions rarely affect commercial airlines. Nevertheless during the autumn and winter months of 2009, 15 weather-related aircraft diversions occurred, all as a result of fog (ATNS 2009). The occurrence of fog at CTIA reduces the arrival rates of aircraft and can result in costly delays.

Van Schalkwyk (2011) verified the visibility forecast in Terminal Aerodrome Forecasts (TAFs) issued at 1200 UTC for CTIA for the period March–August (2004–2007). The purpose of this visibility verification was to determine the quality of these forecasts and to ascertain whether they fall into the thresholds required by ICAO. ICAO, which among other things, concerns itself with safety in aviation, sets high standards for the quality of visibility forecasts, especially when the visibility is less than 1000 m. They require an accuracy of 80% for observed visibilities of 200–700 m (ICAO 2001). Van Schalkwyk (2011) used categorical statistics to verify forecast visibilities in TAFs against observed visibilities at CTIA. Statistical scores such as the probability of detection (POD) and false alarm rate (FAR) were calculated. The TAF issued at 1200 UTC is valid for 24 h starting at 1800 UTC and provides the forecaster with the last and best opportunity to predict the onset of fog for that evening. At that time the latest afternoon atmospheric sounding would also be available. This TAF forms an important part of inbound airlines' fueling strategy for the evening in case of possible diversions. The POD of fog days with a visibility below 1000 m was only 17%, while the FAR was 0.67. These results indicate that fog with visibilities of less than 1000 m was forecast poorly as it was often not foreseen when it did happen (POD = 17%) while when it was forecast it did not happen nearly 70% of the time (FAR = 0.67). This indicates a need for the improvement of fog and visibility forecasts at CTIA and serves as motivation for this research.

One way to address this forecasting concern is to create a better understanding of the characteristics of fog at the airport and the specific conditions under which it occurs. Even though aeronautical summaries (SAWB 1968; SAWS 2010) offer a climatological summary of

general weather that influences CTIA, they do not provide details concerning fog characteristics at CTIA such as fog types, onset and dissipation times, and duration of events. The first approach to the fog forecasting problem is to better understand the various mechanisms involved in its formation, maintenance, and dissipation (Tardif and Rasmussen 2007). Conceptual models have been developed to aid in the forecasting of fog events (Croft et al. 1997; De Villiers and Van Heerden 2007) for specific locations. These conceptual models all include a fog climatology, although other tools such as numerical weather prediction guidance and sounding analysis form part of the conceptual model approach.

The conceptual model or *fog forecasting checklist* for Abu Dhabi International Airport considers the afternoon sounding, forecast minimum temperature, numerical guidance, and synoptic circulation (De Villiers and Van Heerden 2007). However, each model developer has emphasized that the different components of the conceptual model should not be used in isolation and stressed the importance of understanding the climatological characteristics of fog. Meyer and Lala (1990) described how the increased understanding of local climatological parameters associated with a specific fog type benefited the forecasting of fog while Hyvärinen et al. (2007) described the benefit of climatology to aviation forecasters who are responsible for a large number of aerodrome forecasts in varying climatological regions.

The identification of different synoptic types associated with fog forms part of a number of fog-forecasting processes worldwide. Until recently the Australian Bureau of Meteorology (BOM) used the Generalized Analog Statistics Model (GASM), which employed the current synoptic analysis and NWP projections of future weather conditions for comparison with similar past events, obtained from a climate database (Miao et al. 2012). In response to requests from the Federal Aviation Administration (FAA), Tardif (2004) used National Centers for Environmental Prediction–National Center for Atmospheric Research (NCEP–NCAR) reanalysis data (Kalnay et al. 1996) to investigate the synoptic circulation patterns that lead to fog over the northeastern part of the United States, focusing specifically on patterns resulting in fog in the New York region. After using clustering techniques to obtain more information about the nature of fog at three different airports in Finland, 40-yr European Centre for Medium-Range Weather Forecasts (ECMWF) Re-Analysis data (Uppala et al. 2005) were used to visualize the average synoptic situations of the different clusters (Hyvärinen et al. 2007). In this study, self-organizing maps (SOMs) were used as a data reduction technique to determine synoptic circulations that are most frequently associated with fog at CTIA.

The aim of this paper is to facilitate the improvement of fog forecasts at CTIA by elucidating the characteristics of fog at CTIA and providing aviation forecasters with a detailed description of the types of fog that frequently occur and the synoptic circulations associated therewith. This is the first study of its kind and provides operational forecasters with much more detail than previous climatologies for CTIA. As fog events are infrequent and poorly forecast, a synoptic climatology and improved knowledge of the regional characteristics conducive to fog between the months of March and August would provide forecasters with empirical guidance as to the likelihood of fog. The fog climatology results for CTIA are presented here with particular emphasis on identification of the fog type, diurnal characteristics, and synoptic circulation.

2. Definitions

a. Fog and fog event

In South Africa the coding of visibility for aviation purposes is provided in meters or kilometers. A weather observer is obliged to report fog (FG) when the obstruction to vision consists of water droplets or ice crystals and the visibility has been reduced to less than 1000 m. Mist (BR) is reported when the obstruction, due to ice crystals or water droplets, reduces the visibility to at least 1000 m but not more than 5000 m (ICAO 2010). This coincides with the international definition of fog of a horizontal visibility below 1 km in the presence of suspended water droplets (Glickman 2010). Conforming to this definition of fog, any reference made to fog in this paper refers to a reduction in visibility below 1000 m.

Meyer and Lala (1990) indicated the advantage of describing fog events rather than fog days, since synoptic phenomena are not confined to time boundaries. Tardif and Rasmussen (2007) define a fog event as one where fog occurs and lasts for three or more consecutive hours with an observed surface visibility of less than 1600 m, and at least one observation of a surface visibility of less than 1000 m. The same approach is followed here; however, instead of using a maximum visibility threshold of 1600 m as the highest visibility for a fog event, provision was made for variations in visibility of up to 5000 m. This exception was made to prevent separation of a single fog event into two or three shorter events by temporary improvements or fluctuations in visibility.

b. Fog-type definitions

More than one process may be at work during the formation of fog: advection of temperature or moisture

TABLE 1. Definitions and formation mechanisms of radiation, advection, and cloud-base-lowering fog types.

Fog type	Definition in current study–necessary conditions for fog in the hour prior to onset	Formation mechanisms	References
Radiation: fog that develops during the nighttime when light winds, clearing cloud cover, or cloud-free conditions permit maximum radiational cooling and inherently the condensation of moisture	Wind speed less than 3 m s^{-1} prior to onset under cloud-free conditions or the first trace of cloud with a base below 183 m (600 ft) during the hour prior to onset to account for fog building to the surface; lifting cloud bases prior to formation under a prevalent cooling trend before onset	Radiative cooling over a land surface	Meyer and Lala (1990); Pilié et al. (1975); Tardif and Rasmussen (2007)
Advection: a ''wall'' of fog that reaches the observation station characterized by a sudden drop in visibility and appearance of a low cloud base	Sudden onset of fog with wind speeds of 3 m s^{-1} or more and cloud-base height below 600 ft	Mixing caused by the advection of different air masses of contrasting temperatures as moist, warm air comes in contact with a colder water or land surface	Baars et al. (2003); Tardif and Rasmussen (2007)
Cloud-base lowering: fog initially moves in as low-based cloud	Lowering of cloud bases within a 5-h period prior to fog onset, with initial cloud base of 1000 m (3281 ft) or lower	Moistening and cooling of subcloud layer due to cloud-top radiation	Baars et al. (2003); Pilié et al. (1979); Tardif and Rasmussen (2007)

can play a role in the formation of radiation fog, while radiative cooling can be a factor in the formation of other fog types (Tardif and Rasmussen 2007). This has led other authors like Willet (1928) to define up to 11 different types of fog. Since the use of hourly data places limitations on the accurate classification of so many fog types, Tardif and Rasmussen (2007) broadly defined five fog types that frequently affect the New York City region.

Adapting their fog-type classification procedure, this paper will consider three different types of fog: radiation fog, advection fog and fog resulting from the lowering of cloud bases or cloud-base-lowering fog (CBL). Investigations of surface observations showed that morning evaporation fog and precipitation fog (Tardif and Rasmussen 2007) do not occur at CTIA and were not considered in the fog-type classification process. In this paper, fog types are classified according to the primary formation mechanisms at work at the time of onset. These characteristics are summarized in Table 1.

3. Data and methodology

a. Surface observations

Van Schalkwyk (2011) identified the fog season at CTIA from March to August and only data for these winter months were used in the analysis. The type of fog occurrence, as well as the diurnal characteristics of fog events, was investigated by using only hourly aviation routine weather reports (METARs) for CTIA. These data were only available for the 14-yr period from 1997 to 2010, but data for the year 2000 were incomplete and removed completely from the dataset. Official South African Weather Service (SAWS) METAR data were downloaded from Weather Underground (2010). These hourly observations contain information about wind direction and speed, temperature and dewpoint temperature, visibility, cloud amount, and cloud-base height.

b. Fog-type classification

In their study of fog in the New York City region, Tardif and Rasmussen (2007) examined randomly selected fog events and subjectively determined the primary fog formation mechanism for each. From the observations in the 5-h period leading to fog onset, they deduced rules and thresholds that could be applied to other fog events. Based on their results, they developed an objective method of assigning a type of fog to each event using a decision tree designed to identify the primary fog formation mechanism. Where fog events did not meet the classification criteria or insufficient data in the hours leading up to the onset of fog prevented a classification, the event was classified as unknown.

Their hierarchical fog-type classification algorithm was adapted by excluding criteria for precipitation and evaporation fog. Fog events at CTIA were henceforth objectively classified into three different fog types based on conceptual models of their primary formation

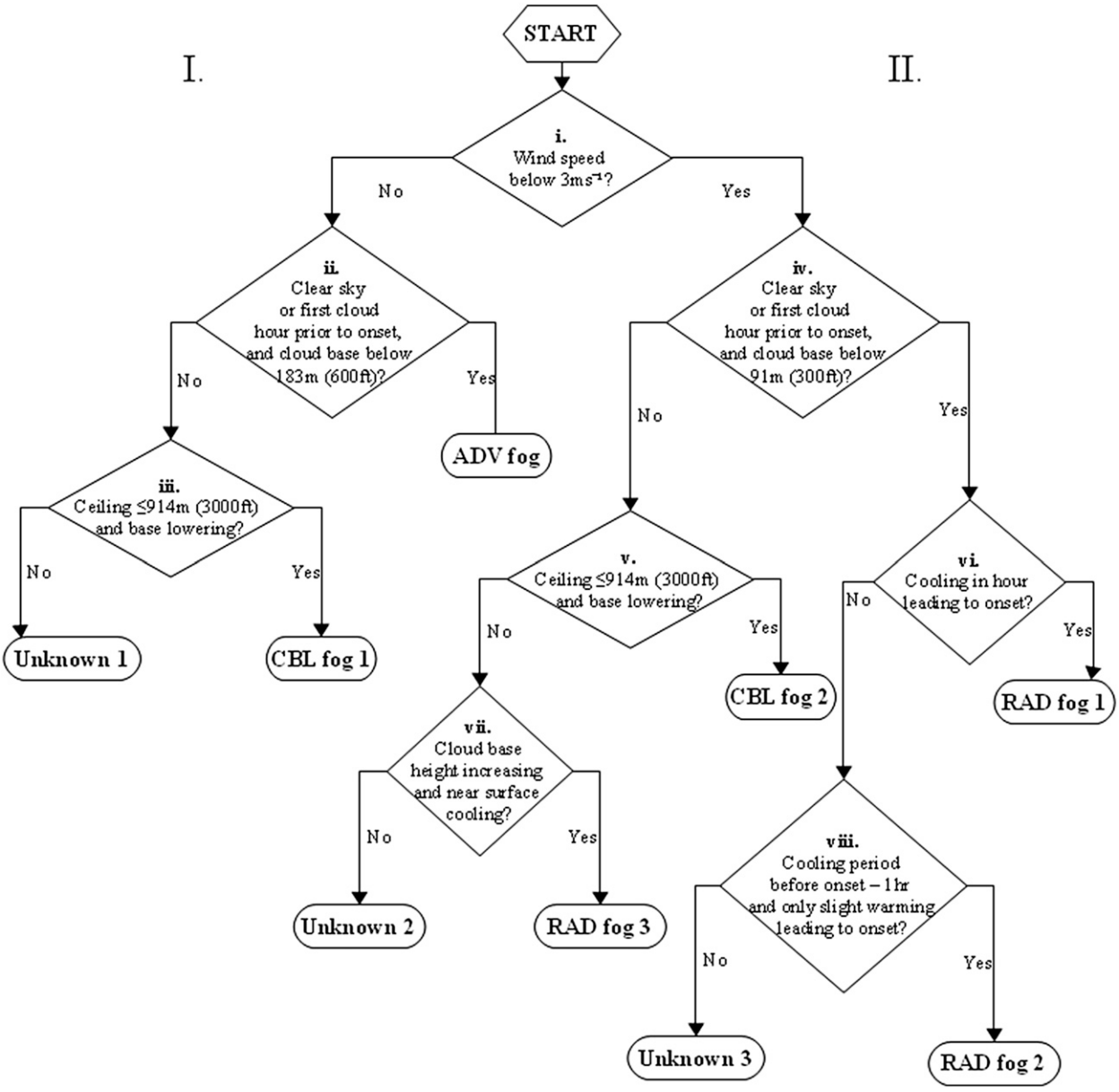

FIG. 2. Decision tree illustrating the fog-type classification method. [Adapted from Tardif and Rasmussen (2007).]

mechanisms (Table 1). The algorithm's decision process is illustrated with the decision tree in Fig. 2. Events that did not match the criteria for classification into one of the three different fog types were classified as unknown. The decision tree in Fig. 2 classifies fog types into two main categories (I and II) depending on whether the wind speed at the time of fog onset t was below 3 m s^{-1} (I) or more than 3 m s^{-1} (II). This essentially distinguishes radiation fog from advection fog (Table 1). Thereafter, the primary mechanisms (i–viii in Fig. 2) considered in the formation of fog at CTIA are shown.

If the wind speed at t was equal to or more than 3 m s^{-1} (i in Fig. 2), cases were classified as either advection, cloud-base-lowering, or unknown events (1 in Fig. 2). To establish whether there was a sudden onset of fog, as is the case with advection events, clear skies or traces of low cloud with bases below 183 m (600 ft) had to be present in the hour before onset (ii in Fig. 2). CBL fog 1 was associated with a drop in cloud base over a period of 5 h prior to fog onset with an initial cloud base equal to or less than 914 m (3000 ft) (iii in Fig. 2).

If the wind speed at t was less than 3 m s^{-1} (i, Fig. 2), the case was classified as a cloud-base-lowering, radiation,

or unknown event (II, Fig. 2). CBL fog 2 has the same definition as CBL fog 1 (iii, Fig. 2), but also occurs under circumstances where the wind speed is less than 3 m s^{-1} (v in Fig. 2). In the absence of cloud cover or with traces of very low cloud bases <300 ft (iv in Fig. 2), three scenarios were investigated to quantify the occurrence of radiation (RAD) fog: RAD fog 1 accounts for radiation events that occur under cloudless conditions at CTIA with dropping air temperatures prior to onset (vi in Fig. 2). RAD fog 2 accounts for radiation events that are associated with cooling in the 4-h period prior to onset, and slight warming in the hour leading to onset (viii in Fig. 2). RAD fog 3 events represent circumstances where cloud cover was present below 914 m (3000 ft) at the time of fog onset (v, Fig. 2), but cloud bases were increasing while the surface temperature was dropping (vii in Fig. 2). Although radiation fog events by definition only take place at night, the decision tree does not test whether the fog onset time was within the hour prior to sunset and before sunrise. Results, however, show that all events classified as radiation fog occurred at night.

Once all 248 events were classified as radiation, advection, or CBL fog, certain characteristics were determined, such as the time of onset and dissipation, event duration, and minimum visibilities associated with the fog event.

c. Synoptic classification

The artificial neural network system of SOMs is described in detail by Kohonen (2001). SOMs provide a mechanism for visualizing a collection of atmospheric states after dominant modes within a dataset were identified (Tennant and Hewitson 2002). The SOM technique identifies representative nodes spanning the data space so that individual data elements may be associated with a node. This means that in a synoptic climatology every synoptic circulation pattern is associated with one of the nodes. Hewitson and Crane (2002) provided detailed information on how SOMs could be used to create a synoptic climatology. Unlike most clustering algorithms, a SOM makes no assumptions about the distribution of the data (Hewitson and Crane 2002) but attempts to identify nodes within a given data space so that the nodes represent the observed distribution (Tennant and Hewitson 2002). The process begins by subjectively choosing the number of nodes after which the reference vectors of the nodes in the SOM array are initialized using random numbers. The SOM calculates the similarity between each data record and each of the node reference vectors. The reference vector of the node that best represents the data record is consequently modified by a user-defined factor, or learning rate. The SOM is trained twice; during the first training process random input vectors are used, which produces a first set of nodes. During the second training of the SOM, the node vectors identified during the first training process are used as the input vectors. In this manner the SOM provides a simplification to a small number of archetypes (Hewitson and Crane 2002). When applying this technique to circulation patterns, the node maps represent physical spatial patterns. The SOM places similar circulation types close to each other and very different types far apart in the SOM space. The nodes represent a nonlinear distribution of overlapping, nondiscreet, circulation types. Each node in a SOM represents a group of similar synoptic circulations that were present in the original dataset.

In this study, SOMs were chosen as the synoptic typing method since they reproduce the climatological synoptic circulation patterns well. Furthermore, each day can be related to a synoptic type and frequencies of types as well as their relation to a meteorological variable, in this case fog, can be easily determined. (Reusch et al. 2005).

The size of the SOM array is determined by the user. In this case 35 nodes (7×5 grid size) were chosen to minimize the degree of generalization that will be produced by the SOM. By choosing more nodes, the representation of detail will be finer and with fewer nodes there will be a broader level of generalization (Hewitson and Crane 2002). It was found that using 35 weather patterns, or a 7×5 grid size, was sufficient to capture the range of synoptic conditions that influence CTIA during winter. Choosing a 7×5 SOM also ensured that the frequency of the number of daily synoptic circulation patterns associated with each of the 35 weather patterns or nodes was similar.

The daily sea level pressure at 0000 UTC for the months of March and August were categorized into 35 archetypal synoptic circulation nodes representing the surface synoptic circulations that occur most frequently during this time of the year. Since the onset of fog events at CTIA generally occurred during the nighttime (six advection events and one CBL event had an onset time after sunrise and before sunset), the 0000 UTC [0200 South African standard time (SAST)] synoptic circulation was chosen as the synoptic circulation closest to the time of fog onset. Apart from the cases where fog onset was after sunrise, this ensured that the most representative synoptic type at the time of fog onset was selected.

Reanalysis II data of daily mean sea level pressure (MSLP) fields at 0000 UTC were obtained from the NCEP/Department of Energy dataset (Kalnay et al. 1996) for all days during March–August of 1997–2010, except for 2000. The data had a 2.5° grid resolution and

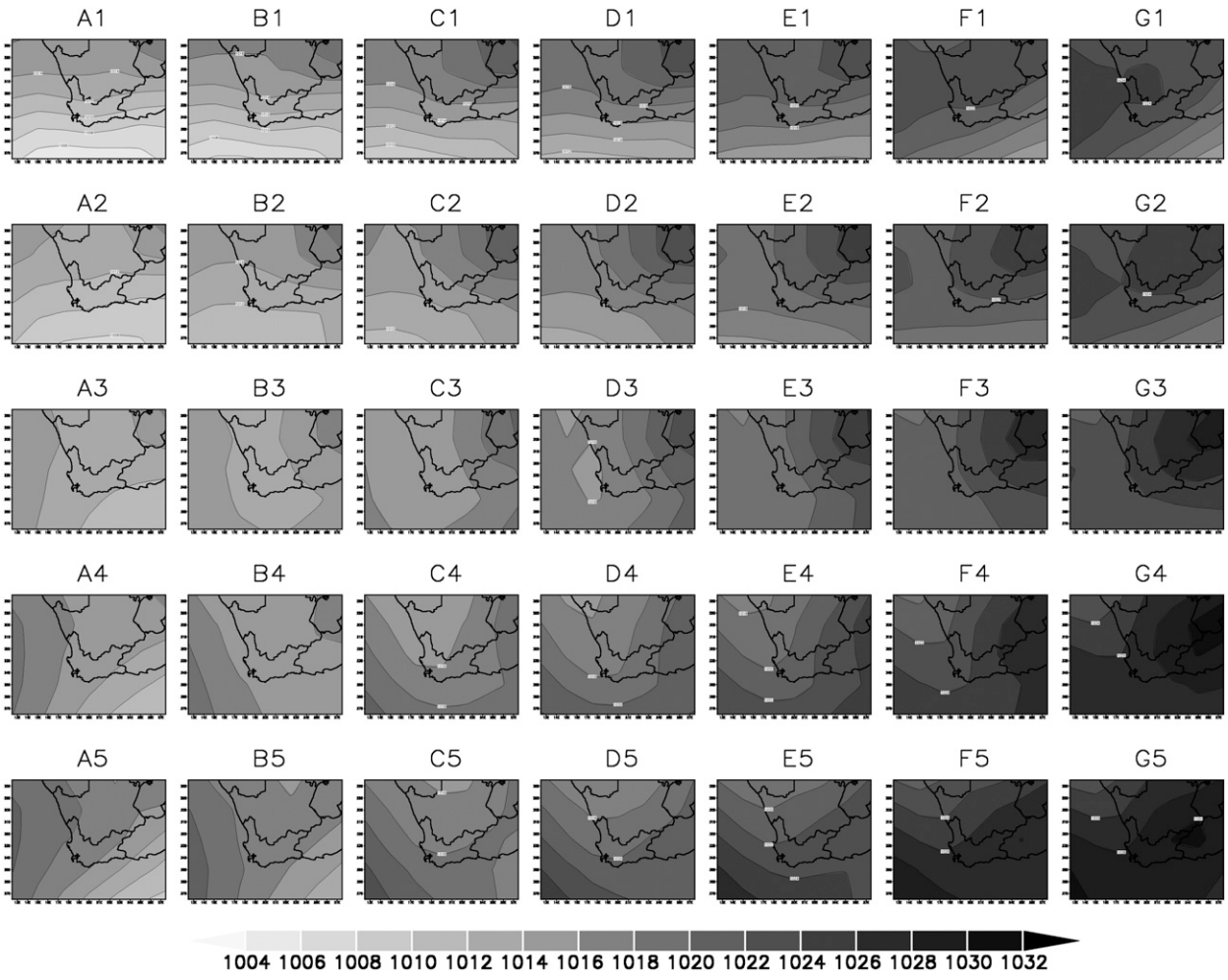

FIG. 3. The 5 × 7 SOM of SLP (mb) from March to August (1997–2010, except 2000) centered around the southwestern Cape. Lighter shades of gray denote regions with lower pressure values while darker shades indicate regions of higher pressure. Similar synoptic types are located adjacent to one other, while dissimilar synoptic types are found at opposite ends of the SOM.

spanned a domain centered around the southwestern Cape (20°–40°S, 10°–35°E). Data are for the 13-yr fog season period from March to August (1997–2010, except 2000).

The reanalysis data were used to create the 7 × 5 SOM by applying SOM software, which is freely available online (http://www.cis.hut.fi/research/som-research) and is referred to as SOM_PAK (Kohonen et al. 1996). First NCEP data were extracted for the domain used in this study. The SOM_PAK system requires that the data used to train the SOM are available in array. The 0000 UTC SLP data from NCEP for the domain used in this study were written into separate arrays for all March–August days from 1997 to 2010. There were data available for 2392 days to train the SOM. The output from the SOM_PAK software was a file that made available the node into which each day used to train the SOM was placed. The data points representing the synoptic pattern for any particular day were placed in the node where the data were most similar to the reference vector of the node. This output file was henceforth further analyzed to create a monthly frequency of fog occurrence as well as the occurrence of different types of fog per node.

To produce a synoptic climatology, the synoptic circulation patterns were related to the fog days over the 13 seasons. Of the 248 events classified as fog, 234 fog days (94%) were identified in the nodes (Fig. 3) to see which surface synoptic circulation patterns were frequently associated with radiation, CBL, and advection fog (Table 2).

Since only one variable (in this case the type of fog associated with a fog event) could be matched with a date and a 0000 UTC synoptic circulation, days where

TABLE 2. Number of fog events mapped to the SOM in Fig. 3 and the relative frequency of fog events as a proportion of the overall number of node occurrences, excluding the 30 events with an unknown classification.

Fog type	No. of events	Relative frequency (%) out of total No. of node occurrences	Corresponding nodes
Radiation	123	5.14	All nodes except A1, B1, C1, A4, and E5
CBL	54	2.26	All nodes except A1, B1, C1, E1, D4, F4, G4, and G5
Advection	27	1.13	C1, D1, E1, A2, B2, D2, E2, F2, A3, C3, E3, F3, G3, C4, C5, and D5

two fog events occurred were manually inspected and preference was given to fog events that were not classified as unknown. This accounts for the 14 events that were not mapped to a node. Finally, the different fog types were related to each of the 35 synoptic circulation patterns.

4. Results

a. Fog types

After application of the hierarchical fog-type classification method in Fig. 2, 92% of all events were classified as radiation, CBL, or advection fog. The other 8% were classified as unknown. This is a similar percentage to the 5% of fog events that remained unclassified in Tardif and Rasmussen's (2007) study. Radiation fog is the most frequent fog type at CTIA (51% of all fog events), followed by CBL fog (27%), and finally advection fog (14%).

Figure 4 expresses the frequency of the different types of fog as a percentage of the total number of fog events that occurred. A striking feature in Fig. 4 is the seasonality of the different types of fog that occur at CTIA during the fog season. Most radiation fog events (in future radiation events) occur during the coldest and wettest part of the season and when nights are longest (June and July). The frequency of radiation events increases from March to June, decreasing slightly in July and August. Few radiation events occurred during March, the only month when radiation events are not most prevalent. A possible explanation for the low number of radiation events at the start of the fog season is that longer daytime hours inhibit sufficient cooling of the boundary layer to become saturated, or it may be due to a lack of surface moisture (CTIA receives rain in winter, from April to September). CBL fog events occur most frequently in May, after which a considerable decrease in the frequency of events is observed toward August (Fig. 4). CBL events are more frequent during the start of the fog season (March–May). Most advection events occur in April. Pure advection events that set in as a ''wall'' of fog occur less frequently than advection events, where the fog layer starts off as low cloud and gradually builds down to the surface to reduce the visibility to below 1000 m. The previous fog climatology (SAWB 1968) conducted at CTIA identified advection fog as the primary fog type at the airport. These results indicate that radiation fog has the highest frequency

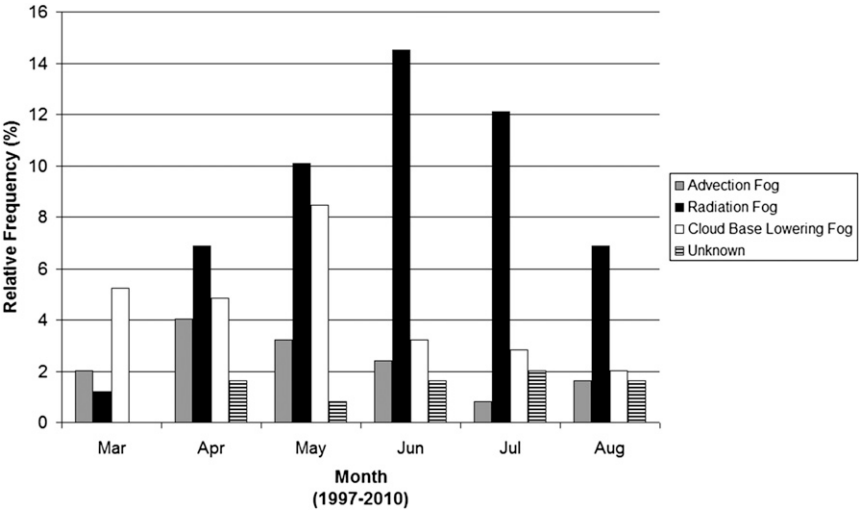

FIG. 4. Monthly frequency of fog types at CTIA from March to August (1997–2010, except 2000).

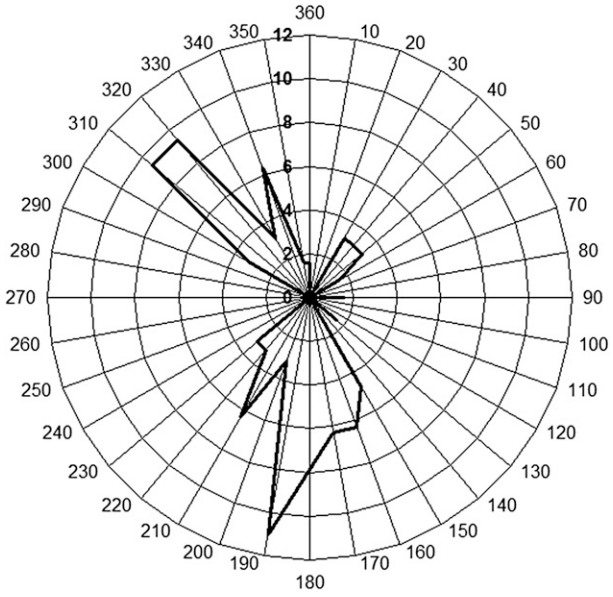

FIG. 5. Frequency of wind direction at the onset of advection fog events from March to August (1997–2010, except 2000).

during all months except March. Advection fog has the lowest frequency of all fog types in every month.

The frequency of wind directions of fog types classified as CBL 1, ADV, and UNKNOWN 1 are shown in Fig. 5. These are the fog events where the surface wind speed is greater than or equal to 3 m s^{-1} at the time of onset. Fog or low cloud is frequently advected toward the airport from Table Bay, located to the northwest of CTIA, and False Bay, located to the south (Fig. 1). The frequencies of fog onset with a southerly wind component are slightly higher than with a northerly component. This could be a direct result of differences in the origin of the air mass in which fog develops: the cold Benguela Current flowing along the west coast of South Africa results in lower sea surface temperatures in Table Bay than in False Bay, where warmer water is found due to intrusions of the warmer Agulhas Current (Demarcq et al. 2010).

FOG-TYPE CHARACTERISTICS

By distinguishing between fog types, the forecaster may better specify the anticipated conditions expected to improve the POD and reduce the FAR. A distribution of the minimum visibility associated with the three main fog types at CTIA is shown in Fig. 6. A visual comparison between the box-and-whiskers plots for the minimum visibility of the three main fog types at CTIA (Fig. 6) shows that radiation fog events tend to have lower visibilities than CBL and advection events. The nonparametric Mann–Whitney test, also known as the Wilcoxon rank sum test, was used to explore the null hypothesis that all groups of data (surface visibility of the various fog types) have the same median at the 95% confidence level (Steyn et al. 1994). The test was performed on various combinations of the groups, with results indicating that distributions can be considered to be significantly different at the 95% confidence level, except when radiation and CBL fog is compared. Seventy-five percent of all three fog types' minimum visibilities were at or below 500 m. This is a very important

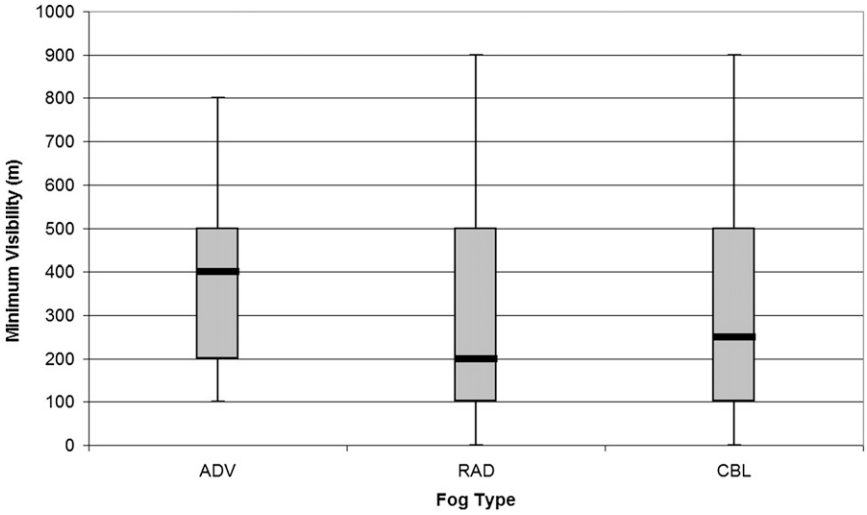

FIG. 6. Box-and-whiskers plots illustrating the distribution of minimum visibility during fog events for each fog type from March to August (1997–2010, except 2000). Gray boxes denote 25th–75th percentiles, while the solid black bar indicates the median value. The vertical lines (whiskers) extend to the maximum and minimum values. The median visibility for ADV fog events was significantly different from RAD and CBL at the 95% level.

TABLE 3. General characteristics of radiation, CBL, and advection fog at CTIA (1997–2010, except 2000). Information is provided about the minimum visibility, duration, onset, and dissipation of fog. Here, Avg = average, Std dev = standard deviation, Me = median and n = number of events. Statistically significant differences are indicated in boldface.

Fog type	Min visibility (% of observations)	Duration (h)	Onset before (−) or after (+) sunrise (*s*)	Dissipation before (−) or after (+) sunrise (*s*)
RAD n = 125	75% ≤ 500 m	4–8	4–9 h before *s*	Mostly at sunrise
	50% ≤ 200 m	Me = 5	**Earlier onset time than ADV and CBL**	Between 4 h before *s* and 2 h after *s*
	25% ≤ 100 m	Avg = 6	Avg = −6.3 h	Avg = −1.2 h
	Avg = 315 m	Std dev = 3.12	Std dev = 3.9 h	Std dev = 3.6 h
	Std dev = 244.3 m		—	—
	Lower visibility than ADV		—	—
CBL n = 59	75% ≤ 500 m	4–9	2–7 h before *s*	Mostly after *s*
	50% ≤ 250 m	Me = 6	Avg = −3.6 h	Between 1 h before *s* and 3 h after *s*
	25% ≤ 100 m	Avg = 7	Std dev = 5 h	Avg = 0.8 h
	Avg = 328 m	Std dev = 3.3	—	Std dev = 3.3 h
	Std dev = 256.2 m		—	—
	Lower visibility than ADV		—	—
ADV n = 28	75% ≤ 500 m	4–9	Between 8 h before *s* and 6 h after *s*	Mostly 2 h before *s*
	50% ≤ 400 m	Me = 6	Avg = −0.1	Between 5 h before *s* and 2 h after *s*
	25% between 100 and 200 m	Avg = 6	Std dev = 7.6 h	Avg = −0.6 h
	Avg = 414 m	Std dev = 2.6	**Later onset than CBL fog**	Std dev = 4.2 h
	Std dev = 213.8 m		—	—

factor to consider when issuing minimum visibility forecasts associated with fog, since verification results of fog days between March and August (2004–07) show that only 17% of fog days with a minimum visibility below 1000 m were forecast in advance (Van Schalkwyk 2011). The distributions of event duration of the three different fog types (not shown) were also tested with the Mann–Whitney test and it was found that no significant difference exists between the duration of different fog events.

The reduction in visibility and the duration as well as the time of onset and dissipation associated with different fog types are some of the important characteristics aviation forecasters need to be aware of to improve fog forecasts. These characteristics for the three main fog types at CTIA are summarized in Table 3. Information about the duration of different fog types and their related minimum visibilities is supplemented by additional information about the time of fog onset and dissipation. The time of sunrise at CTIA was rounded up or down to the closest hour: 0500 UTC during March, April, May, and August and 0600 UTC during June and July (South African standard time is UTC +2 h).

All fog types showed a tendency to form at night and dissipate during daytime, CBL events had a tendency to start later in the night than radiation fog, but advection fog events tended to start closest to sunrise (Table 3) Advection events had a larger variation in onset times than radiation and CBL events. In contrast to radiation and CBL events, advection events sometimes had an onset between 9 and 12 h after sunrise (not shown). This equates to an onset time between 1400 and 1800 UTC, which is the late afternoon and early evening at CTIA. A marine fog layer will often remain stationary along the coast during daytime as solar heating of the landmass causes dissipation of the fog by convective mixing that takes place between drier and warmer continental air and the advancing marine layer. But as soon as temperatures start to decrease, the cooler and less turbulent boundary layer allows an inland propagation of the fog layer (Tardif and Rasmussen 2007), allowing for fog onset during the late afternoon and early evening.

A Mann–Whitney test found a statistically significant difference at the 99% confidence level between the onset time of advection and CBL fog events and radiation events. Similarly, it was found that the onset time of advection fog is later than the onset of CBL fog, at a 95% confidence level.

In most cases fog dissipated at or after sunrise (Table 3), but some fog events dissipated prior to sunrise. Meyer and Lala (1990) explain that high dissipation rates of fog shortly after sunrise is a result of increased solar radiation, which enhances mixing via localized heating. But from a fog forecasting point of view, an event that dissipates earlier than expected can lead to forecast errors just as much as an event that dissipates much later.

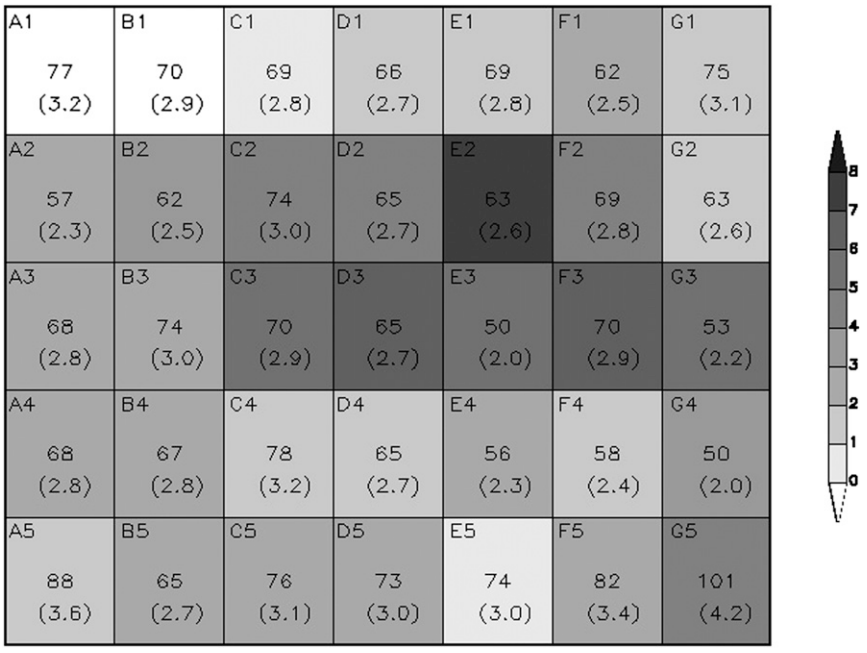

FIG. 7. The numbers in each block are the total numbers of days that were mapped to each node and the numbers in parentheses are the relative frequencies (%) of occurrence of each node. The shading denotes the relative frequency (%) of fog in each node, i.e., the number of fog events per node as a proportion of the total number of fog events.

Forecasting the dissipation time of radiation events that clear before sunrise is challenging since the reasons behind clearance before sunrise are often unclear. However, this shows that dissipation of fog is not always due to an increase in solar radiation, but could also be ascribed to a change in the low-level horizontal advection during evolving synoptic conditions.

The tendency of fog to dissipate before sunrise was observed most often with advection and radiation fog events with an average dissipation time of 1 h prior to sunrise (Table 3). CBL events generally clear after sunrise and a Mann–Whitney test found a statistically significant difference at the 95% (90%) confidence level between the dissipation time of CBL and advection (radiation) events. A Mann–Whitney test confirmed that there is no statistically significant difference between clearance times of radiation and advection fog events.

b. Synoptic circulations

In Fig. 3 similar synoptic types are located adjacent to one other, while dissimilar synoptic types are found at opposite ends of the SOM. The synoptic types representing westerly troughs (most likely associated with the passage of cold fronts) are in the top portion of the SOM. Consider the first line in the SOM and note how the westerly systems gradually move southward with a high pressure system establishing itself over the western interior at G1. Generally lower pressures are found on the left but with increasing pressures to the right. Nodes B3 and C3 look similar, but in C3 the central pressure of the low–trough is slightly higher than in B3. Synoptic types with a dominant high over the interior are found in the nodes to the right, while synoptic types with lower pressure over the interior and a high to the west of the country are found in the bottom-left corner. Transition states, mainly featuring areas of lower pressure along the west coast, are found in the center nodes.

Matching the fog events with their respective synoptic types provides insight into the circulation patterns mostly associated with fog at CTIA. The frequency of occurrence of a synoptic circulation associated with all fog events, irrespective of the type of fog, is illustrated in Fig. 7. The nodes associated with most fog events at CTIA are nodes E2, D3, and F3, which all illustrate an area of lower pressure along the west coast with a high pressure pattern dominant over the interior (Fig. 3).

Nodes A1 and B1 were the only nodes not associated with any fog event. These nodes represent the synoptic circulations associated with the passage of cold fronts, which are the most common source of rainfall for the southwestern Cape during the winter months (SAWB 1996). In comparison to the nodes that were associated with fog events at CTIA, the contour spacing between

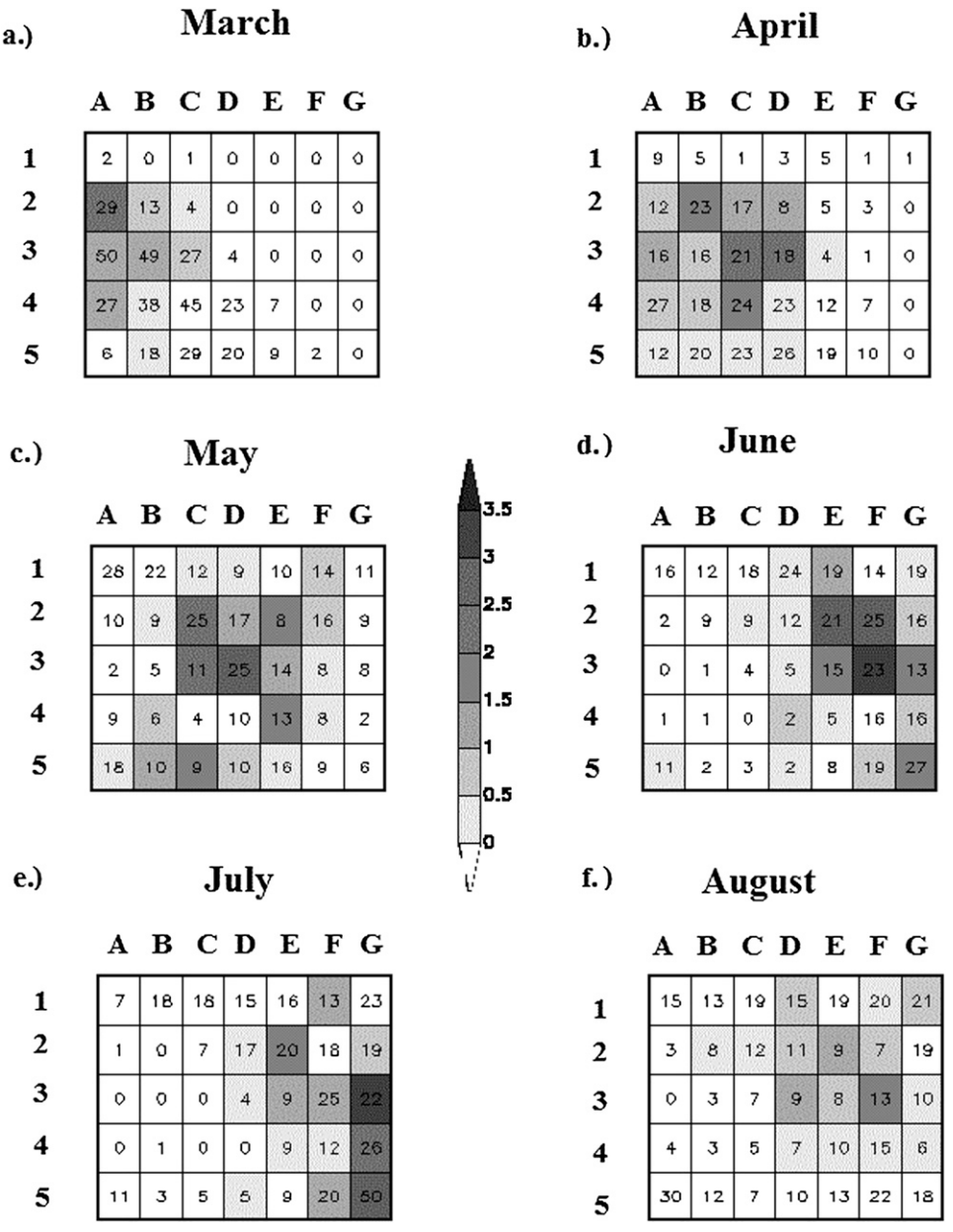

FIG. 8. The numbers in each block are the total numbers of days that occurred in that particular month per node and the shading denotes the relative frequency (%) of fog in each month per node relative to the total number of fog events.

isobars in nodes A1 and B1 is smaller. This signifies a tighter pressure gradient, which would result in stronger winds at the surface. The SLP in the vicinity of CTIA in node A1 is 1010 hPa, which is the lowest pressure out of all the nodes in Fig. 3.

1) MONTHLY FOG SYNOPTIC CIRCULATIONS

Advective processes are the main cause of fog at the start of the fog season, with the highest frequency of advection fog in April, but in the middle of winter (June) radiative processes are the most common cause of fog with a noticeable decrease in the number of advection and CBL events toward July and August.

A monthly analysis of the frequency of synoptic types associated with fog (Fig. 8) shows a gradual change between March and August. Figure 8 not only illustrates the seasonal shift of fog-related synoptic types, it also shows the shift of synoptic types in general from the left-hand side of the SOM in March to the right-hand side in August. Consider node E2, for example, which was

TABLE 4. Nodes with the highest number of fog events for the months March–August (1997–2010, except 2000) and relative frequency of fog associated with each node as a proportion of the total number of fog events.

Month (1997–2010)	Node No.	No. of fog events associated with node	Relative frequency (%)
Mar	A2	5	2.1
Apr	C3 and D3	5 + 5	2.1 + 2.1
May	D3	6	2.6
Jun	F3	8	3.4
Jul	G3	8	3.4
Aug	F3	4	1.7

associated with the most fog events at CTIA (Fig. 7). The synoptic pattern associated with this node never occurred in a March month. It did occur 5 times in April but was not associated with any fog events. The node occurred most often in June when it was associated with fog approximately 3% of the time. Fog events at the start of the fog season occurred most frequently on the left-hand side of the SOM (Fig. 8a). Thereafter, a gradual shift is observed in the shades of gray depicting the frequency of fog events from synoptic types in column A in March (Fig. 8a), to columns C–E in April and May (Figs. 8b and 8c), and to columns F and G in June–August (Figs. 8d–f).

Table 4 provides a summary of the nodes that received most fog events on a monthly basis during the fog season. These nodes all display a region of lower pressure along the west coast with a dominant high over the interior of South Africa. Node A2 (Fig. 3), which has the highest number of fog events in March, is different from the other synoptic types associated with fog from April to August. In March, a coastal low is present along the south coast of South Africa, resulting in an onshore circulation pattern with a westerly wind component over the western interior. Maritime air is advected toward CTIA after passing over the cold Benguela Current along the west coast. A comparison with Fig. 4 shows that CBL and advection fog occur more frequently in March than radiation fog does. The apparent onshore circulation in node A2 provides moisture for the formation of fog during this month. The west coast trough in nodes C3 and D3 (Fig. 3) is the predominant synoptic type associated with fog during April months (Table 4). The central pressure of the low pressure system increases from B to D in row 3 (Fig. 3). Weak pressure gradients with only a 2-hPa pressure difference in node D3 are present without an obvious onshore component, although an east-to-southeasterly circulation pattern around the periphery of the trough can advect moist air in from the south over False Bay. In Fig. 4 it can be seen how radiation fog events start to increase in association with these weak gradients. The west coast trough (node D3) is still the dominant fog synoptic type in May when radiation fog starts to occur more frequently (Fig. 4). The trough southwest of the country is slightly weaker and the high over the central interior is stronger than the circulation during March. Thus, air of continental origin progressively comes more into play toward the middle and end of the fog season. From June to August the trough along the west coast becomes less dominant than the high over the interior of South Africa. Consider nodes F3 and G3 (Fig. 3), which occur most frequently when fog occurs between the months of June and August. Here, the west coast trough lies to the west of the subcontinent and the high over the interior has strengthened to 1028 hPa. Weak gradients over the Cape Peninsula contribute to radiative cooling at nighttime, and from Fig. 4 it can be seen that radiation fog occurs more frequently than any other type of fog.

2) FOG TYPES RELATED TO SYNOPTIC CIRCULATION

(i) Radiation fog

Out of the 35 nodes, 30 were associated with radiation fog at one time or another (Fig. 9a). A comparison of the total frequency of fog events (Fig. 7) with the radiation fog frequency (Fig. 9a) shows that similar nodes had the highest frequency in each case, although a significantly lower frequency of radiation fog events can be seen on the left-hand side of Fig. 9a. From Fig. 9a it is clear that radiation fog is favored by synoptic types with a strong high over the interior (central pressure greater than 1022 hPa) and a weak trough (less than 2-hPa pressure difference) along the west coast of South Africa (Fig. 7). The highest number of radiation events was associated with nodes from columns C to G and rows 2 and 3 (Table 5). Six percent of the overall 8% fog events that were associated with node E2 (Fig. 7) were associated with radiation fog (Fig. 9a) and node E2 was associated with radiation fog 17% of the time when the synoptic type occurred.

In node E2 (Fig. 3) a weak coastal low is present along the southwest coast of South Africa. This results in a westerly-to-northwesterly onshore wind component at CTIA. As mentioned in section 2b, a combination of advective and radiative processes can often lead to the formation of fog. In this case the coastal low advects moisture toward CTIA during the afternoon, after which radiative processes take over at night, especially with the dominant high over the interior (Fig. 3), eventually resulting in the formation of radiation fog. Willet (1928) described fog that formed as a result of these two processes as ''maritime fog'' due to the maritime origin

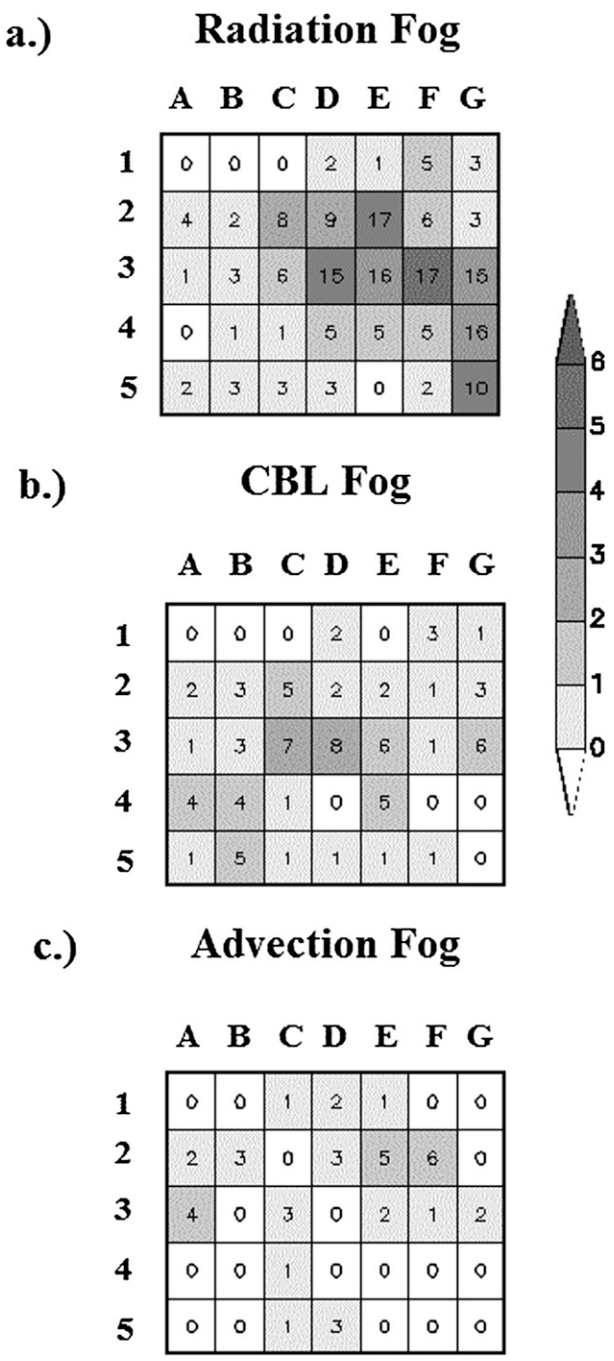

FIG. 9. The numbers in each block are the percentage of days with fog expressed relative to the total number of days in that node and the shading denotes the relative frequency (%) of fog for each fog type relative to the total number of fog events.

of surface moisture. This type of fog is also known as ''advection–radiation fog'' and has been found to be a common occurrence in the coastal plains of the state of New Jersey (Tardif and Rasmussen 2007). Advection–radiation fog also occurs in the southern and central United States when moist, warm air from the Gulf of Mexico is advected over progressively colder and slightly elevated land (Ahrens 2000). Baars et al. (2003) indicated that advection–radiation fog was one of the most common causes of fog at Los Angeles International Airport, occurring when the sea breeze advects moisture toward the airport during afternoons. The synoptic circulation pattern represented by node E2, as well as the fact that most fog events associated with E2 were classified as radiation fog according to primary formation mechanisms, suggests that advective and radiative processes combine to produce fog at CTIA.

TABLE 5. Nodes with the highest number of radiation, CBL, and advection fog events (March–August, 1997–2010, except 2000) and relative frequency as a proportion of the total number of fog events.

	Node	No. of fog events associated with node	Relative frequency (%)
RAD	F3	12	5.1
	E2	11	4.7
	D3	10	4.3
	G5	10	4.3
CBL	C3	5	2.1
	D3	5	2.1
	C2	4	1.7
ADV	F2	4	1.7
	E2	3	1.3
	A3	3	1.3

(ii) CBL fog

Twenty-seven of the 35 synoptic circulation types in Fig. 3 were associated with CBL fog (Fig. 9b). Most CBL events were associated with nodes from columns B to E and rows 2 and 3 (Table 5). Nodes C3 and D3 (Fig. 3) show similar circulation patterns with broad regions of lower pressure along the west coast. They were also associated with the most fog events during April and May (Table 4), when CBL fog frequently occurs (Fig. 4). The easterly circulation pattern around the southern periphery of the low in C3 and D3 most likely advected moisture and low stratus cloud westward toward CTIA. Node C2 (Fig. 3) indicates the presence of a coastal low to the southwest of CTIA. In this case the source of moisture would be a result of a westerly-to-northwesterly onshore component, as opposed to the easterly component in the other two nodes.

(iii) Advection fog

Sixteen nodes in Fig. 3 were associated with advection fog. Figure 9c indicates the distribution of these nodes. Most advection events were concentrated in columns D–F of row 2 (Fig. 9c). A few advection events were associated with nodes in column C. The nodes that were associated with the highest number of advection events

are shown in Table 5. Nodes F2 and E2 lie adjacent to each other in the SOM (Fig. 3) and represent similar synoptic circulation patterns, both of which indicate a coastal low along the southwest coast with a dominant high over the interior. Node A3, however, indicates the low along the south coast with the start of a new ridging process by the Atlantic Ocean high from the west. In Fig. 5 it was shown that most fog events with a wind speed greater than 3 m s^{-1} at the time of onset have either a southerly or northerly wind direction. This is confirmed by the synoptic circulation patterns in nodes F2 and E2 (Fig. 3), which show a westerly-to-northwesterly onshore circulation pattern along the southwest coast, while the circulation in node A3 would be associated with a southerly wind component at CTIA.

(iv) Nodes E2 and D3

Of all the nodes represented in Fig. 3, nodes E2 and D3 were associated with the most fog events at CTIA. The monthly breakdown of synoptic types in Fig. 8 shows that the synoptic circulation represented by node E2 occurs most frequently in June and July but rarely in March and April. Out of the 63 times that node E2 appeared (Fig. 7), it was associated with fog on 17 occasions (not shown), which implies a 1 in 4 chance of fog at CTIA under similar synoptic conditions.

Node D3 was associated with a similar number of radiation events as node E2 (Table 5) but accounted for radiation events that took place during the first part of the fog season, occurring most often during April and May (Fig. 8).

The main difference between nodes E2 and D3 is the region of lower pressure along the west coast in node D3, while the low pressure pattern is farther to the south in node E2 with a high pressure pattern over the interior. CBL fog occurred with node D3 (five events) and node E2 (three events), but advection fog occurred only once with node E2 and advection fog rarely occurs toward the end of the fog season (Fig. 4).

5. Summary and conclusions

The aim of this research was to provide aviation forecasters at CTIA with a comprehensive overview of the types of fog that frequently affect the airport, the characteristics of the different fog types, and the synoptic circulation associated therewith. The hierarchical classification method successfully identified fog events into three different fog types: radiation fog, CBL fog, and advection fog. It was shown that radiation fog is the most frequent fog type at CTIA. This is in contradiction to previous findings, which attributed most fog to advection processes.

Making use of SOMs, it was shown that radiative and advective processes often combine to form radiation fog at CTIA. The interaction of the coastal low on the southwest coast and high over the interior of South Africa is important in the formation of fog at CTIA. The shallow low advects moisture onto the Cape Flats during the day while the high over the interior causes subsidence, which allows radiation fog to form at night when temperatures decrease.

The results of this research could be applied to facilitate the improvement of the forecasting process of fog events at CTIA. Aviation forecasters at CTIA should carefully consider the possibility of fog formation between March and August, especially on evenings where there are no limiting factors for the formation of fog (such as rain or strong winds). Since the primary formation mechanisms of fog vary during the course of the fog season, the fog types associated most frequently with a particular month (Fig. 4) should be taken into consideration during the forecasting process.

Once forecasters are familiar with the most likely fog type for a specific month, the expected mean sea level pressure synoptic circulation at 0000 UTC should be assessed by using numerical weather prediction (NWP) models. The forecast synoptic circulation, as well as the central pressures associated with the highs and lows, should be compared with those of the nodes that caused fog at CTIA most frequently (see Table 5). Forecasters should bear in mind that similar circulation types may cause different types of fog depending on the month of the season.

If the synoptic circulation seems favorable for the development of fog, the expected fog type can be determined by making use of the same characteristics that were used to classify fog types in Fig. 2. Once the forecaster has reached a conclusion about the expected type of fog, the duration, minimum visibility, and time of onset and dissipation can be inferred from the results in Table 3, which can be used to produce a TAF.

Acknowledgments. The authors thank the three anonymous reviewers for their constructive comments that helped improve the manuscript.

REFERENCES

ACSA, cited 2010: Cape Town International Airport, aircraft statistics. Airports Company South Africa. [Available online at www.acsa.co.za.]

Ahrens, C. D., 2000: *Meteorology Today.* Brooks/Cole, 528 pp.

ATNS, 2009: New radar statistics. Air Traffic and Navigation Services Standard Rep. ATM DIR 4/2009, ATM DIR 5/2009, and ATM DIR 7/2009.

Baars, J. A., M. Witiw, and A. Al-Habash, 2003: Determining fog type in the Los Angeles basin using historic surface observation

data. Preprints, *16th Conf. on Probability and Statistics in the Atmospheric Sciences/13th Symp. on Global Change and Climate Variations,* Long Beach, CA, Amer. Meteor. Soc., J3.8. [Available online at https://ams.confex.com/ams/pdfpapers/29133.pdf.]

Carter, T. J., 2005: The evolution of coastal lows along the south coast of South Africa. M.S. dissertation, Dept. of Geography and Environmental Studies, University of Zululand, KwaDlangezwa, South Africa, 165 pp.

Civil Aviation Authority, 2007: Operations specifications template. Form CA ACC-F-011. [Available online at www.caa.co.za.]

Croft, P. J., R. L. Pfost, J. M. Medlin, and G. A. Johnson, 1997: Fog forecasting for the southern region: A conceptual model approach. *Wea. Forecasting,* **12,** 545–556.

Demarcq, H., R. G. Barlow, and F. A. Shillington, 2010: Climatology and variability of sea surface temperature and surface chlorophyll in the Benguela and Agulhas ecosystems as observed by satellite imagery. *Afr. J. Mar. Sci.,* **25,** 363–372, doi:10.2989/18142320309504022.

De Villiers, M. P., and J. Van Heerden, 2007: Fog at Abu Dhabi International Airport. *Weather,* **62,** 209–214.

Glickman, T., Ed., 2000: *Glossary of Meteorology.* 2nd ed. Amer. Meteor. Soc., 855 pp.

Hewitson, B. C., and R. G. Crane, 2002: Self-organizing maps: Applications to synoptic climatology. *Climate Res.,* **22,** 13–26.

Hyvärinen, O., J. Julkunen, and V. Nietosvaara, 2007: Climatological tools for low visibility forecasting. *Pure Appl. Geophys.,* **164,** 1383–1396.

ICAO, 2001: International standards and recommended practices: Attachment E. Annex 3 to the Convention on International Civil Aviation, International Civil Aviation Organization.

——, 2010: Technical specifications related to meteorological observations and reports: Appendix 3. Annex 3 to the Convention on International Civil Aviation: Meteorological Service for International Air Navigation, 17th ed. International Civil Aviation Organization, APP 3-1–APP 3-5.

Kalnay, E., and Coauthors, 1996: The NCEP/NCAR 40-Year Reanalysis Project. *Bull. Amer. Meteor. Soc.,* **77,** 437–471.

Kohonen, T., 2001: *Self-Organizing Maps.* 3rd ed. Springer, 511 pp.

——, J. Hynninen, J. Kangas, and J. Laaksonen, 1996: SOM_PAK: The Self-Organizing Map Program package. Laboratory of Computer and Information Science Tech. Rep. A31, Helsinki University of Technology.

MeteoGraphics, 2010: Terra3D visualization software with bing terrain layer. MeteoGraphics. [Available at www.meteographics.de.]

Meyer, M. B., and G. G. Lala, 1990: Climatological aspects of radiation fog occurrence at Albany, New York. *J. Climate,* **3,** 577–586.

Miao, Y., R. Potts, X. Huang, G. Elliott, and R. Rivett, 2012: A fuzzy logic fog forecasting model for Perth Airport. *Pure Appl. Geophys.,* **169,** 1107–1119, doi:10.1007/s00024-011-0351-x.

Olivier, J., and J. Van Heerden, 1999: The South African Fog Water Collection Project. Water Research Commission Rep. 671/1/99., 149 pp. [Available from Library and Publications Division, Private Bag X03, Gezina 0031, South Africa.]

Pilié, R. J., E. J. Mack, W. C. Kocmond, C. W. Rogers, and W. J. Eadie, 1975: The life cycle of valley fog. Part I: Micrometeorological characteristics. *J. Appl. Meteor.,* **14,** 347–373.

——, ——, ——, ——, and U. Katz, 1979: The formation of marine fog and the development of fog-stratus systems along the California coast. *J. Appl. Meteor.,* **18,** 1275–1286.

Reusch, D. B., R. B. Alley, and B. C. Hewitson, 2005: Relative performance of self-organizing maps and principal component analysis in pattern extraction from synthetic climatological data. *Polar Geogr.,* **29,** 188–212.

SAWB, 1968: Aeronautical climatological summaries, 1957–1964. WB31, South African Weather Bureau, Pretoria, South Africa, 73 pp.

——, 1996: Regional description of the weather and climate of South Africa: The weather and climate of the extreme southwestern Cape. South African Weather Bureau, Pretoria, South Africa, 39 pp.

SAWS, 2010: Aeronautical climatological summaries, 1996–2010. Cape Town International Airport. CLS-CI-AERO-SUM-FACT-2010.001.2, South African Weather Service, Pretoria, South Africa, 30 pp.

Steyn, A. G. W., C. F. Smit, S. H. C. Du Toit, and C. Strasheim, 1994: *Modern Statistics in Practice.* J. L. Van Schaik, 761 pp.

Tardif, R., 2004: Characterizing fog occurrences in the northeastern United States using historical data. Preprints, *11th Conf. on Aviation, Range, and Aerospace Meteorology,* Hyannis, MA, Amer. Meteor. Soc., P10.6. [Available online at https://ams.confex.com/ams/pdfpapers/81650.pdf.]

——, and R. M. Rasmussen, 2007: Event-based climatology and typology of fog in the New York City region. *J. Appl. Meteor. Climatol.,* **46,** 1141–1168.

Tennant, W., and B. C. Hewitson, 2002: Intra-seasonal rainfall characteristics and their importance to the seasonal prediction problem. *Int. J. Climatol.,* **22,** 1033–1048.

Uppala, S. M., and Coauthors, 2005: The ERA-40 Re-Analysis. *Quart. J. Roy. Meteor. Soc.,* **131,** 2961–3012.

Van Schalkwyk, L., 2011: Fog forecasting at Cape Town International Airport: A climatological approach. M.S. dissertation, Dept. of Geography, Geoinformatics and Meteorology, University of Pretoria, 133 pp.

Weather Underground, cited 2010: Historic METAR data downloads. [Available online at www.wunderground.com.]

Willet, H. C., 1928: Fog and haze, their causes, distribution, and forecasting. *Mon. Wea. Rev.,* **56,** 435–468.

World Airports, cited 2010: Cape Town International Airport, O.R. Tambo International Airport. [Available online at www.azworldairports.com.]